Supplemental Information

A Mechanosensory Circuit that Mixes

Opponent Channels to Produce Selectivity

for Complex Stimulus Features

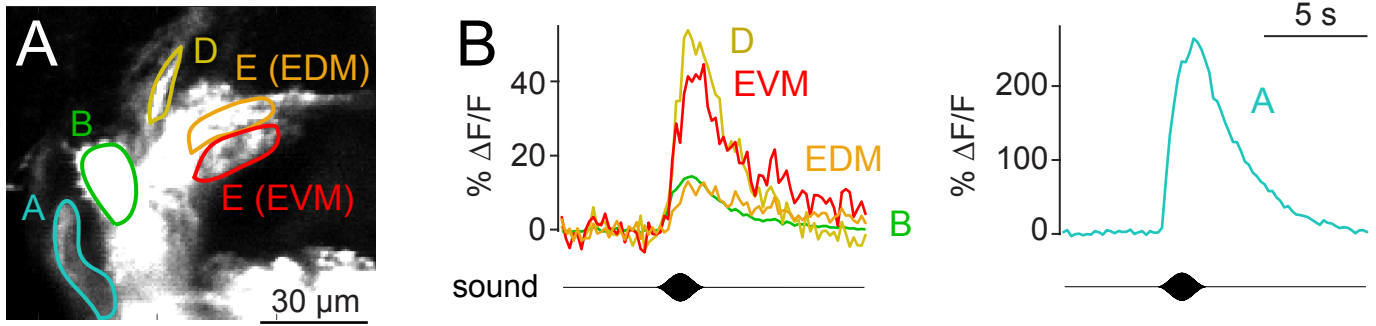Allison E.B. Chang, Alex G. Vaughan, and Rachel I. Wilson

Figure S1, related to Figure 1: Sound responses in JONs.

A) Resting GCaMP6s fluorescence in JON axons in vivo, imaged with a 2-photon microscope. Image is a horizontal optical section viewed from the ventral side (dorsal is up, medial is right). GCaMP is expressed in all JONs under the control of the *pebbled-Gal4* driver. Major branches are outlined. The E branch can be divided into EDM and EVM sectors (Kamikouchi et al., 2006). The C branch is not easily identifiable in this section.

B) Sound responses in indicated branches in this imaging plane. Responses were recorded simultaneously in all branches. Branch A shows the largest responses (note different vertical scale), but all the other branches in this imaging plane also respond. Each trace represents the average of 10 trials. Similar results were obtained in 3 of 3 experiments (in 3 flies). The stimulus is a 200 Hz tone pip, 2 s in duration. Speaker position and sound intensity (~ 20 mm/s) were the same in all the sound experiments in this study.

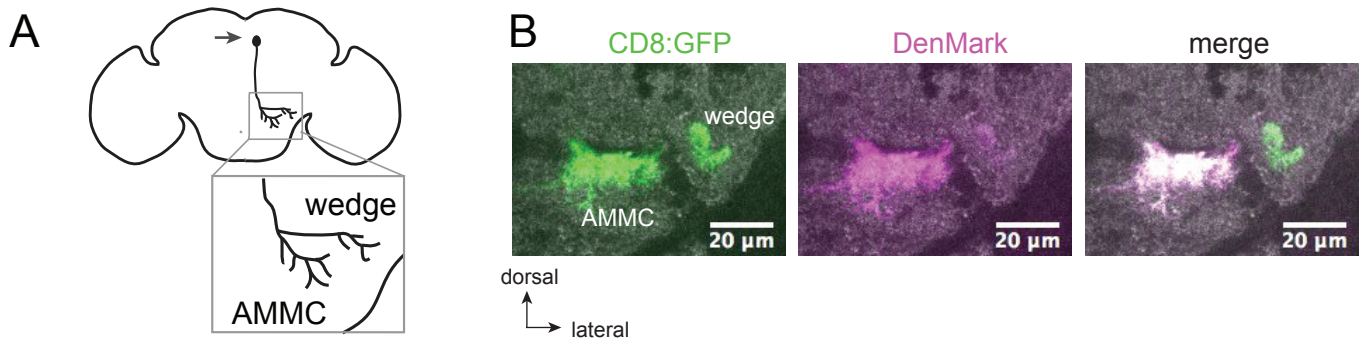Genotype is *pebbled-Gal4/+;20XUAS-IVS-GCaMP6s(attP40)/+*.

Figure S2, related to Figure 1: aPN3 neurons send their dendrites to the AMMC.

A) Schematic of an aPN3 neuron within the brain (coronal view). Arrow indicates the cell body location. The enlarged inset shows processes in the antennal mechanosensory and motor center (AMMC, where JON axons terminate) and in the wedge (a higher-order auditory brain region; Vaughan et al., 2014; Matsuo et al., 2016).

B) aPN3 neurons expressing a membrane marker (green, CD8:GFP) and a dendritic marker (magenta, DenMark). The white channel is neuropil (nc82 immunofluorescence). Image is a projection through a coronal stack. The region circumscribed by the image is similar to the area of the enlarged inset in (A). Note that DenMark localizes to the AMMC but not the wedge. This confirms that the aPN3 neuron processes in the AMMC are indeed dendrites. The same result was also previously reported using an alternative dendrite marker (Vaughan et al., 2014).

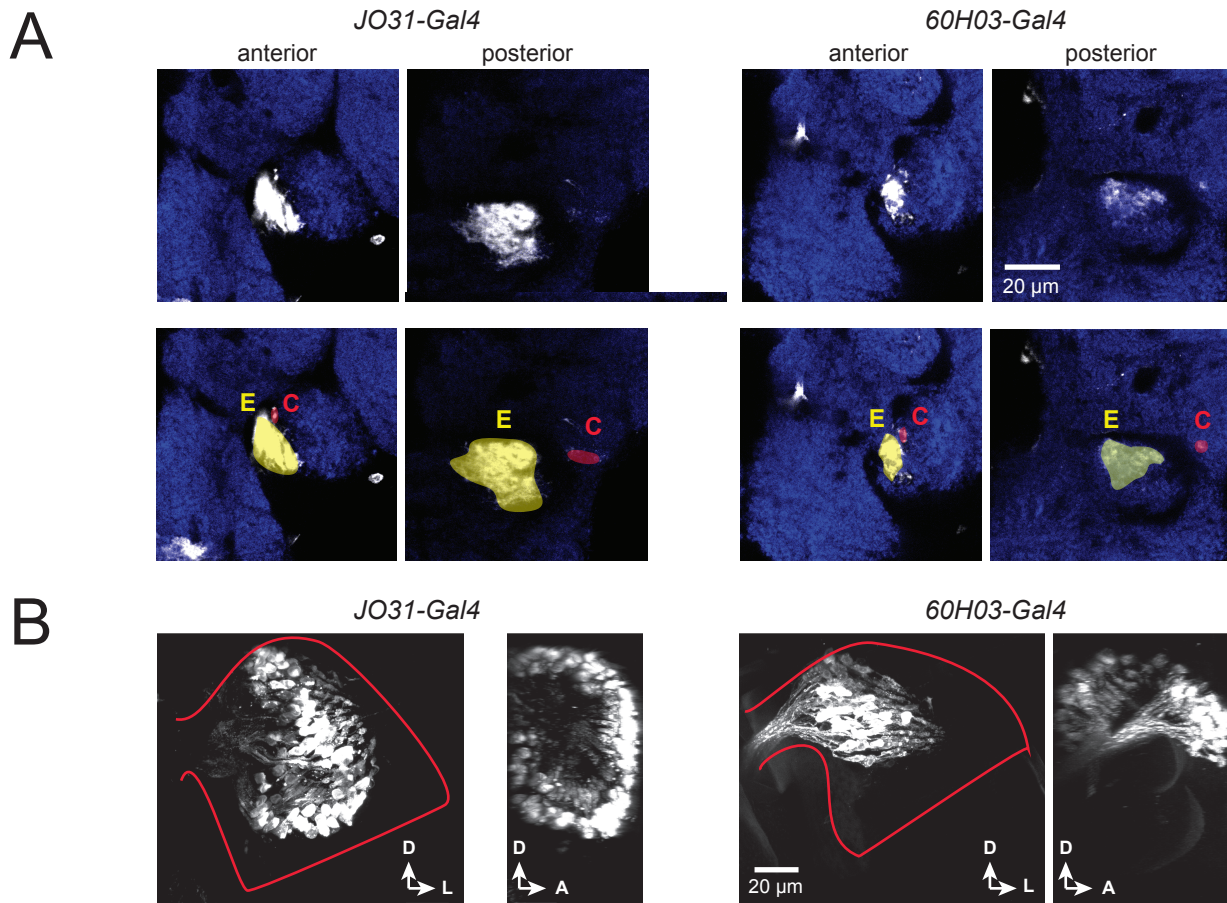Genotype: *UAS-DenMark/+;70G01-Gal4,10xUAS-CD8:GFP/+*.

Figure S3, related to Figure 1: Anatomical comparison between JO31-Gal4 and 60H03-Gal4.

The total number of JONs that express Gal4 in the *JO31-Gal4* line (~193 JONs) exceeds the estimated number of C and E JONs (~137 in total), but the identity of the additional Gal4-expressing JONs in this line is not known (Kamikouchi et al., 2006). Here we show that *60H03-Gal4* drives expression in a smaller group of JONs (~50), and expression in *60H03* appears to be restricted to the C and E JONs.

A) Axons of JONs (white, CD8 immunofluorescence) innervating brain neuropil (blue, nc82 immunofluorescence). Two sections are shown for each genotype, one at the level of the antennal nerve as it enters the brain (anterior), and one just after the point where the E and C JON axons diverge (posterior). The lower row of images is colored to indicated conjectured boundaries of the E and C JON bundles. In total, there are fewer C JONs than E JONs, and so the cross-sectional area of the C JON bundle is smaller (Kamikouchi et al., 2006).

B) JONs in the antenna (white, native GFP fluorescence). Two maximum-intensity projections are shown, one along the anterior-posterior axis (left, outline of the second antennal segment in red) and one along the lateral-medial axis (right). In the latter view, *JO31* labels a ring-like structure, whereas *60H03* labels a smaller cluster of cells on the dorsal side of the ring. We counted an average of 52±9 GFP-positive cells in *60H03* (n=3 antennae; mean ± s.e.m.). Kamikouchi et al. (2006) counted ~193 labeled cells in *JO31*, and that study also estimated that there are a total of ~137 JONs belonging to type C or type E.

Genotypes are *JO31-Gal4/CyO;10xUAS-CD8:GFP* and *60H03-Gal4;10xUAS-CD8:GFP*.
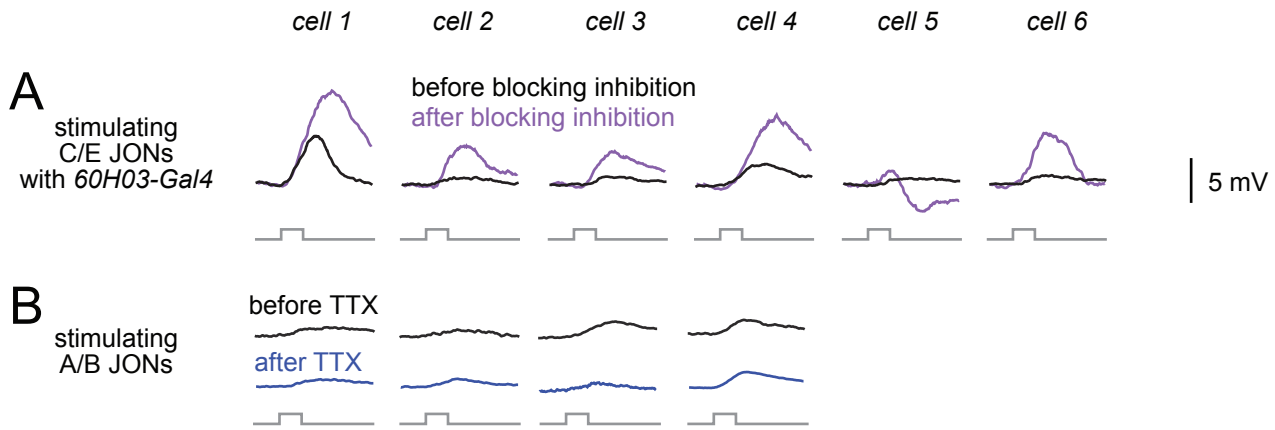
Figure S4, related to Figure 1: aPN3 responses to optogenetic stimulation of JON subsets.

A) aPN3 neuron responses to optogenetic stimulation of C/E JONs that express Gal4 under the control of *60H03* (light pulse is 50 msec, n=6 cells). Results are similar to those shown in Figure 1F for the *JO31-Gal4* line. Blocking synaptic inhibition (with 5 µM picrotoxin and 50 µM CGP54626) revealed excitation in every cell. At the end of each experiment, we added tetrodotoxin (TTX) to the bath (2 µM) to confirm that most of the aPN3 response relied on spiking in JONs; the maximum TTX-insensitive response in any neuron was 2 mV (data not shown). Genotype is *10xUAS-CD8:GFP/20XUAS-IVS-CsChrimson.mVenus(attP40);60H03-Gal4/10xUAS-CD8:GFP,70G01-Gal4*.

B) aPN3 responses to optogenetic stimulation of A/B JONs (n=4 cells). We observed either no response, or a small response that was unaffected by TTX (2 µM). Because these responses are unaffected by TTX, they must not require spiking in JONs, and instead are likely due to light leaking into the head and directly activating aPN3 neurons (which also express CsChrimson). Genotype is *10xUAS-CD8:GFP/20XUAS-IVS-CsChrimson.mVenus(attP40);JO15-Gal4/10xUAS-CD8:GFP,70G01-Gal4*.
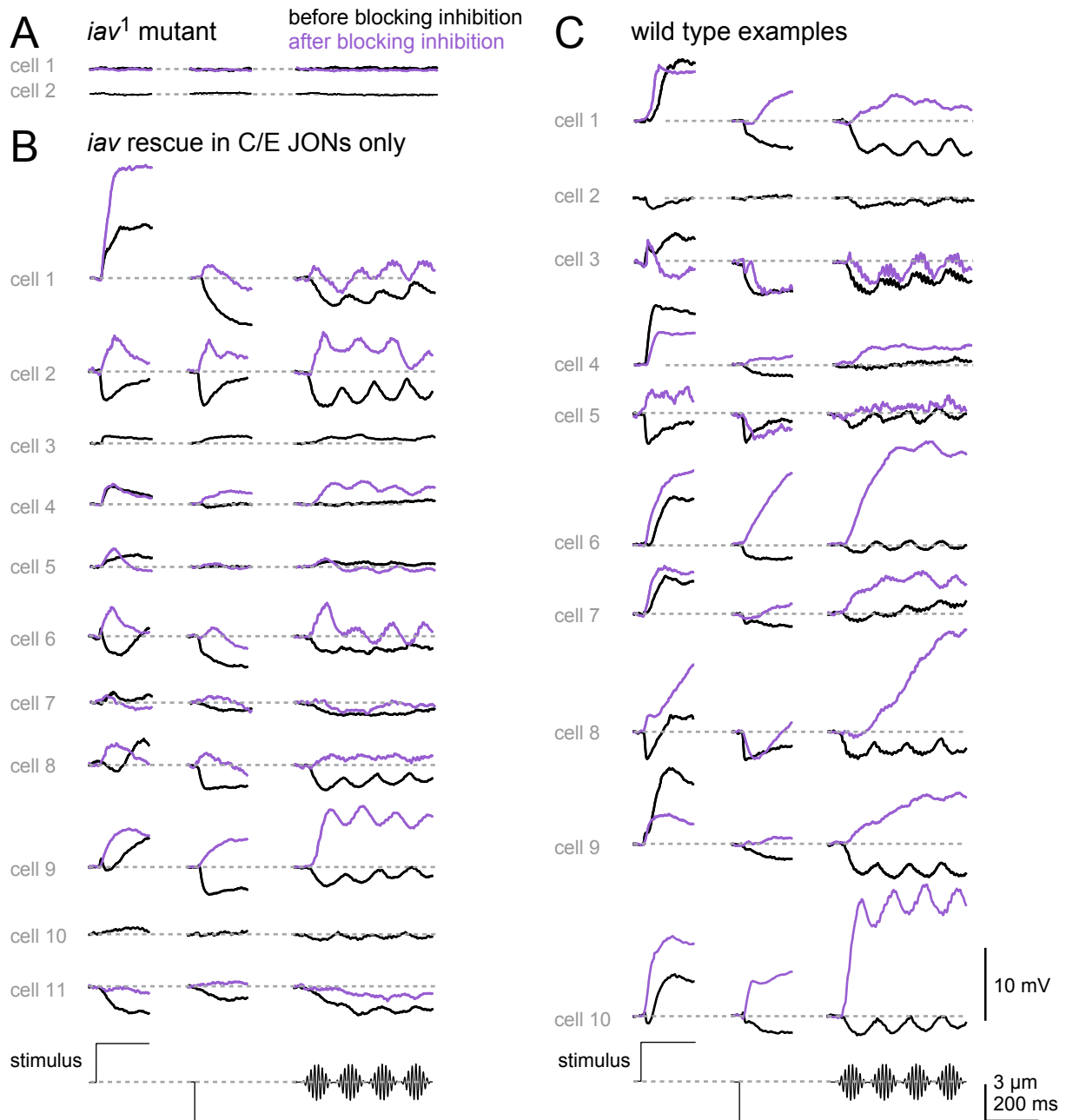
Figure S5, related to Figure 1: C/E JONs are sufficient to confer normal responses on aPN3 neurons.

A) The iav^1 mutation is known to abolish stimulus-evoked responses in JONs (Gong et al., 2004). We recorded from aPN3 cells to confirm that this mutation also abolishes stimulus-evoked responses in these cells, as expected (n=2 cells). These flies were males of the genotype $iav^1;CyO/+;UAS-iav/10xCD8:GFP,70G01-Gal4$. Stimuli were delivered with a piezoelectric actuator in all panels of this figure. In one of these experiments we blocked synaptic inhibition using bath application of picrotoxin and CGP54626, and we still saw no response to the stimulus.

B) In this mutant background, we rescued *iav* expression specifically in C/E JONs under Gal4/UAS control. These flies were males of the genotype $iav^1; JO31/+;UAS-iav/10xCD8:GFP,70G01-Gal4$, and were siblings of the flies in (A). These cells had relatively normal-looking stimulus-evoked responses (n=11 cells). In 9 of these cells we blocked synaptic inhibition, and we found that this had a range of effects, similar to that seen in wild type recordings.

C) An array of wild type responses to the same stimuli are shown for comparison purposes. These flies were females of the genotype 1*0xUAS-CD8:GFP,70G01-Gal4*. These 10 cells are representative of 18 cells we recorded from using these stimuli.

These results indicate that C/E JONs are sufficient to confer normal stimulus-evoked responses on aPN3 neurons, including responses to step displacements and responses to sound-like stimuli. It is difficult to make a meaningful quantitative comparison between genotypes because of the diversity within the aPN3 population; we also do not know whether the level of activity in individual C/E JONs is quantatively normal in the rescue genotype.
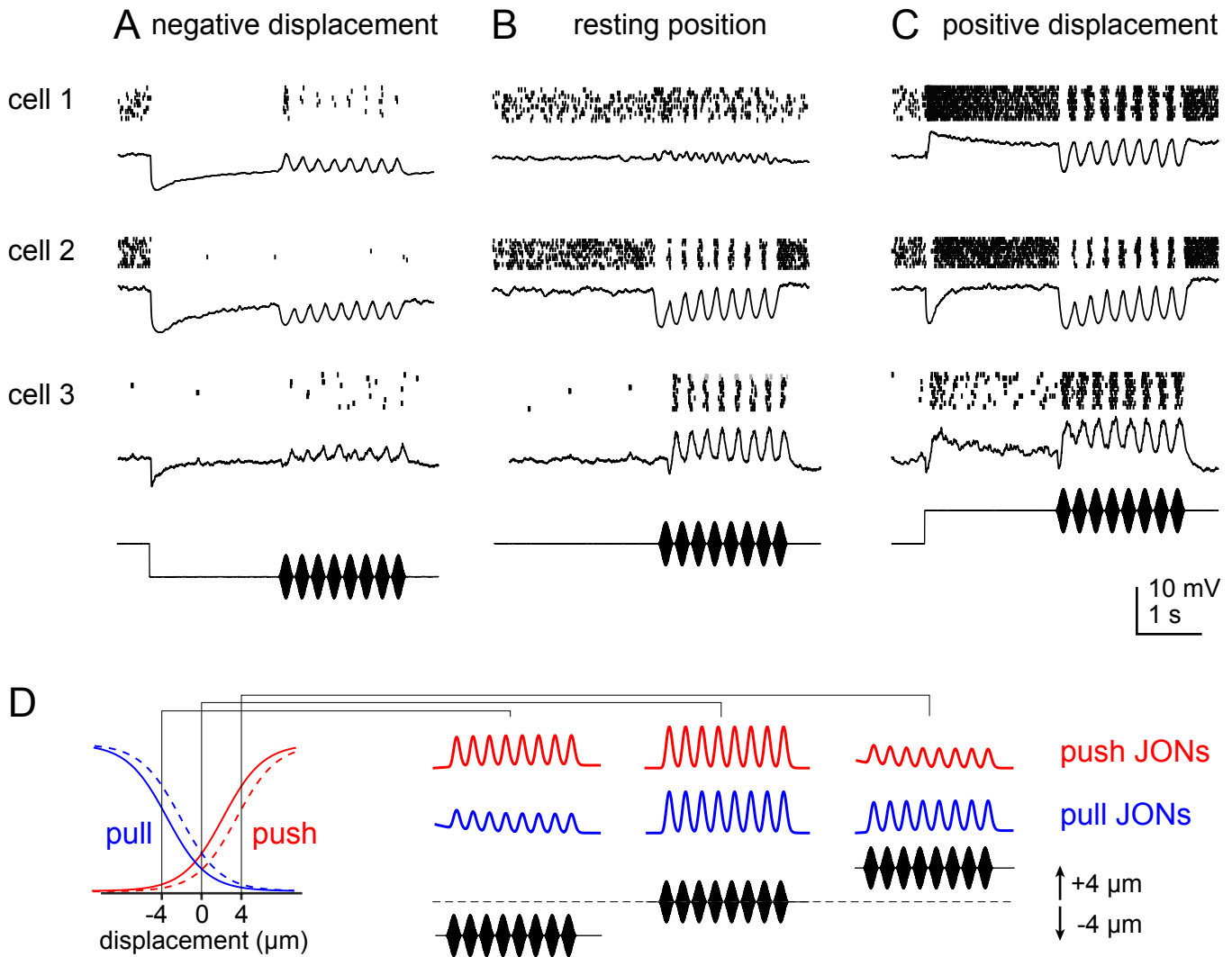
Figure S6: aPN3 neurons can encode sound stimuli from a wide range of resting antennal positions

A-C) A piezoelectric device was used to generate fictive sound stimuli riding on top of a sustained displacement equal to -4 μm, 0 μm, or +4 μm (A, B, or C, respectively). Here we show aPN3 neuron spiking responses (rasters, top) and average voltage (bottom). Each aPN3 neuron generates robust phase-locked sound responses over a limited range of antennal positions, with different cells preferring different positional ranges. For example, adding a negative bias to the antenna's position increases sound sensitivity in cell 1, but decreases sound sensitivity in cell 2. Genotype is *10xUAS-CD8:GFP,70G01-Gal4*.

D) Model JON responses to the same three stimuli. Dashed curves show horizontal shift after adaptation to a +4 μm step. A negative bias decreases the sound sensitivity of pull JONs. This is because a negative bias puts the stimulus into the linear part of the pull JON curve, and so pull JONs now respond more symmetrically to the positive and negative parts of each vibration cycle; as a result, low-pass filtering attenuates the pull JON response, because the positive and negative components tend to cancel each other out. The same thing happens to push JONs when there is a positive bias. Pull and push channels can add either constructively or destructively in different aPN3 neurons, meaning that the sensitivity of an aPN3 neuron to vibration envelope modulations may either increase or decrease when one channel is selectively suppressed by a bias.
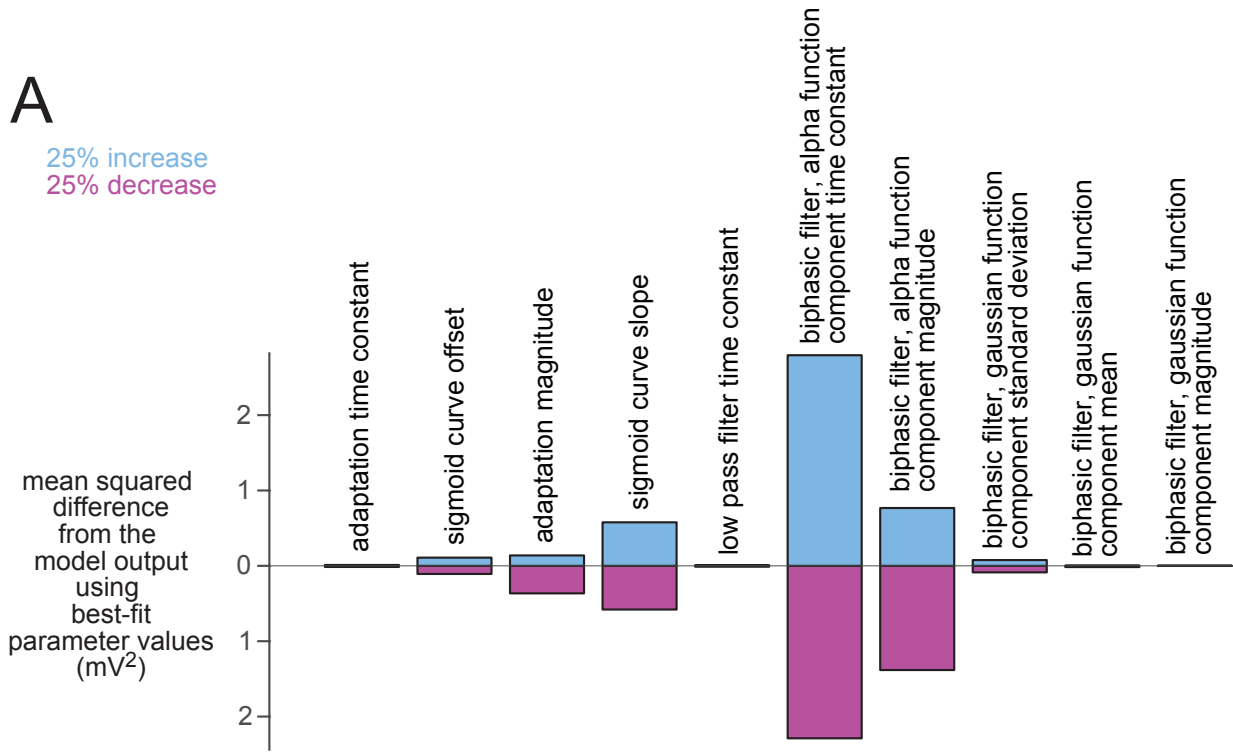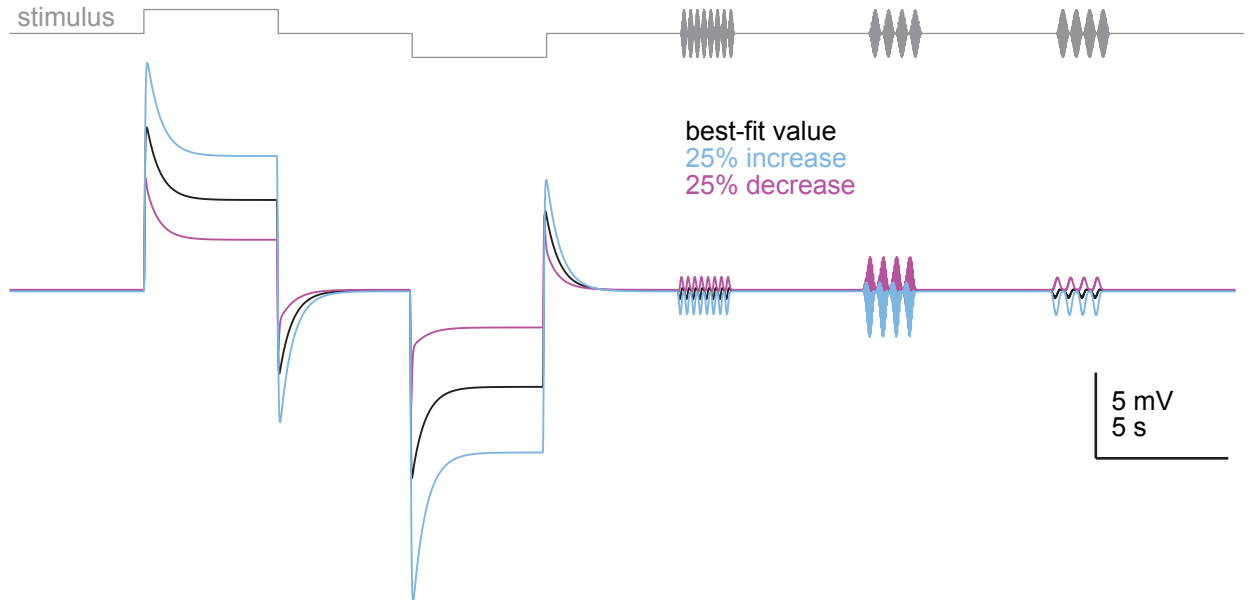
Figure S7, related to Experimental Procedures: Robustness of model output to parameter values.

A) In order to quantify how much the model output changes when its parameters are varied, we individually increased and decreased each parameter by 25%, and we measured how much the model output changed (quantified as the mean squared difference from the model output using best-fit parameter values).

B) Top trace (in gray) shows the stimulus waveform that we used as the input to the model for this exercise (consisting of a positive and a negative step, and three sets of amplitude-modulated sinusoids with different carrier frequencies). Bottom traces show the response of the model using best-fit parameter values (black), or a 25% change in the value of one parameter (the time constant of the alpha function component of the biphasic filter). This is the parameter that has the largest effect on the magnitude of the response.

Supplemental Experimental Procedures

Flies

Experiments were performed in adult *Drosophila melanogaster* using the following genotype: *10xUAS-IVS-CD8:GFP(su(Hw)attP1),70G01-Gal4(attP2).* The exceptions were the experiments in **Figures 1D, 1E, and 1F** (see below), and also where noted in Supplemental Figures. Flies were reared on conventional cornmeal agar medium coated with a thin layer of hydrated potato flakes. Cultures were maintained at 25ºC under a 12h/12h light/dark cycle. All experimental flies were female. Flies were aged 20 to 48 hours post-eclosion (except in **Figure S1**, see below).

Transgenes and mutants

Some of the drivers used in this study have been previously described as follows. *JO31-Gal4* drives expression in C/E JONs, and *JO15-Gal4* drives expression in A/B JONs (Kamikouchi et al., 2006). *70G01-Gal4(attP2)* derives from the Janelia Research Campus FlyLight collection (Pfeiffer et al., 2008) and drives expression in 20 – 24 aPN3 neurons per brain (Matsuo et al., 2016; Vaughan et al., 2014). *pebbled-Gal4* drives strong Gal4 expression in most or all JONs, along with most other peripheral sensory neurons in the antenna, including olfactory receptor neurons, but not in any central neurons in the regions where these afferents terminate (Sweeney et al., 2007).

The UAS transgenes and LexAop transgenes used in this study have been previously described as follows: *10xUAS-IVS-CD8:GFP(su(Hw)attP1)*, *10xUAS-IVS-CD8:GFP(attP40),* and *13xLexAop2-CD8:GFP(attp40)* (Pfeiffer et al., 2010), *20XUAS-IVS-GCaMP6s(attP40)* (Chen et al., 2013), *UAS-FRT-stop-FRT-GFP* (Vlasits et al., 2014), *20XUAS-IVS-CsChrimson.mVenus(attP40)* (Klapoetke et al., 2014), *UAS-DenMark(attP40)* (the DenMark reagent was first described in Nicolai et al., 2010; here we used a variant called *UAS-pJFRC-TLN-cherry* which we received from Gerry Rubin's lab at Janelia Research Campus, and which has been previously published by Kohl et al. 2014), and *iav*[1];;*UAS-iav* (Kwon et al., 2010). *UAS-CD2* was obtained from the Bloomington Drosophila Stock Center (stock 1284).

Two transgenic lines are characterized here for the first time. *70G01-LexA(attP40)* appears to label the same neurons as *70G01-Gal4(attP2)*. *60H03-Gal4(attP2)* drives expression in a subset of C/E JONs (**Figures S3** and **S4**). Both derive from the Janelia Research Campus FlyLight collection (Pfeiffer et al., 2008).

Finally, *iav*[1] flies were obtained from the Montell lab as part of the *iav*[1];;*UAS-iav* stock (Kwon et al., 2010), and also from the Bloomington Drosophila Stock Center (stock 6029). The Bloomington Stock Center allele has recently been renamed iav[hypoB-1] (http://flybase.org/reports/FBrf0230970.html).

Electrophysiology

Whole-cell patch-clamp recordings were performed as previously described (Wilson and Laurent, 2005), with some modifications. Flies were cold-anesthetized, inserted into a hole in a titanium foil platform and secured using UV-curable glue. The top of the fly's head was tilted forward slightly (relative to its natural position) to ensure access to aPN3 cell bodies (which reside on the posterior part of the brain). The ventral and anterior part of the head, the ventral part of the thorax, and the entire abdomen remained dry throughout the dissection and experiment. The antennae were distant enough from the titanium foil that they could rotate freely without any part of the antennae or arista touching the foil. The thorax and posterior face of the head were exposed above the foil and submerged in oxygenated saline. The medial third of the posterior side of the head cuticle was removed to expose the brain. Air sacs and perineural sheath were gently removed with fine forceps to reveal the aPN3 neuron cell bodies, which reside on the posterior face of the brain.

All experiments were performed at room temperature, and the brain was constantly perfused with oxygenated saline containing: 103 mM NaCl, 3 mM KCl, 5 mM TES, 8 mM trehalose, 10 mM glucose, 26 mM $NaHCO_3$, 1 mM NaH_2PO_4, 1.5 mM $CaCl_2$, and 4 mM $MgCl_2$ (pH 7.3, osmolarity adjusted to 270-275 mOsm). The saline was bubbled with 95% O2/5% CO2 and circulated in the bath at ~2-3 ml/min. Cell bodies were visualized using infrared optics and a 40× water-immersion objective on an upright compound microscope (Olympus BX51).

Patch pipettes (9-11 MΩ) were pulled the day of the recording and filled with internal solution containing 140 mM KOH, 140 mM aspartic acid, 10 mM HEPES, 1 mM EGTA, 1 mM KCl, 4 mM MgATP, 0.5 mM Na_3GTP, and 13 mM biocytin hydrazide (pH adjusted to 7.2 ± 0.1, osmolarity adjusted to 265 ± 3 mOsm).

Whole-cell patch-clamp recordings were performed from GFP-labeled aPN3 neuron somata in current-clamp mode using an Axopatch 200B amplifier. Data were low-pass filtered at 5 kHz, digitized at 10 kHz by a 16 bit A/D converter (National Instruments, BNC 2090-A), and acquired in Matlab. Stable mechanosensory responses could be recorded for 1-3 hours. The small amplitude of the spikes in these neurons (~10 mV) is likely due to the spike initiation zone being some distance from the soma (Gouwens and Wilson, 2009). Small amounts of current injected through the patch pipette (±10 pA) had a substantial influence on the spiking behavior of the cells, indicating that our electrode had some control over the voltage at the spike initiation zone. In most experiments, a standing hyperpolarizing current (about -5 pA) was injected to compensate for the depolarizing seal conductance (Gouwens and Wilson, 2009) in order to hold cells between -60 and -50 mV. aPN3 neurons had a high input resistance (approximately 1.5 to 2 GΩ, on average).

Calcium imaging

Calcium imaging in **Figure S1** was performed in female flies obtained by crossing the *pebbled-Gal4* stock with *20XUAS-IVS-GCaMP6s(attP40)*. Flies were aged 9 weeks to increase levels of GCaMP6s expression (Hong and Wilson, 2015; Marella et al., 2006). Flies were prepared as for the electrophysiology experiments, except that the head was rotated 180º relative to the body, so that the ventral side of the head pointed upward toward the microscope objective. This allowed better optical access to JON axon terminals, which are located near the ventral edge of the brain. The dorsal and anterior part of the head, the ventral part of the thorax, and the entire abdomen remained dry throughout the dissection and experiment. The antennae were visually inspected to make sure they could freely rotate without any part of the antennae or arista touching the foil. The ventral part of the head cuticle was then removed to expose the brain, and air sacs were gently removed with fine forceps. The brain was continuously perfused with oxygenated saline during the experiment. Two photon fluorescence of GCaMP6s was excited with 940-nm light and collected with a Bergamo II microscope (Thorlabs). Images were acquired at a resolution of 256×128 pixels and a frame rate of 5.22 Hz. The sound stimulus was presented for 2 s, beginning 10 s after the onset of each imaging trial, for a total of 10 trials, with an 37-s interval between stimuli.

Only the JON axon bundle contralateral to the speaker was imaged; this corresponds to the side of the brain where responses are larger, as one would predict from the geometry of the antennae (Morley et al., 2012). Images were acquired at a z-position near the level of the AP sub-branch of the JON axon bundle (Kamikouchi et al., 2006). This z-plane was selected because the axons of the A, B, D, and E JONs can be clearly delineated at this vertical level, but similar results were observed at other z-levels. Similar results were obtained in three independent experiments in three different flies. We did not attempt to measure signals in C JONs because the C bundle can be difficult to identify when many other JON types are labeled.

The sound-evoked signals we observe in E JONs are intermediate in amplitude between the large signals reported by Mamiya et al. (2015) and the smaller signals reported by Kamikouchi et al. (2009) and Matsuo et al. (2014). These differences likely reflect differences in sound stimulus intensity and the use of different

genetically-encoded calcium sensors. Importantly, the intensity of the sound stimulus, and the position of the speaker relative to the fly's antenna, was the same in our calcium imaging experiments and electrophysiology experiments.

Pharmacology

We used 5 μM picrotoxin and 50 μM CGP54626 to block synaptic inhibition. In *Drosophila*, picrotoxin is an antagonist of GABA-A receptors (Wilson and Laurent, 2005) and GluCl receptors (Liu and Wilson, 2013), and CGP54626 is an antagonist of GABA-B receptors (Wilson and Laurent, 2005). Drugs were bath-applied via the saline perfusate. Picrotoxin was prepared as a concentrated stock solution in aqueous NaCl (140 mM). CGP54626 was prepared as a concentrated stock solution in dimethyl sulfoxide. TTX was prepared as a concentrated stock solution in sodium citrate. Stock solutions were subsequently diluted to the appropriate final concentration in saline immediately before use. In most cases where inhibitory synaptic transmission was blocked, both 5 μM picrotoxin and 50 μM CGP54626 were used. In a minority of cases, only 5 μM picrotoxin was used. Because data from both conditions appeared identical, they were pooled. Where this is the case, it is denoted as "5 μM picrotoxin with or without 50 μM CGP54626." In cases where both drugs are always used in combination, it is denoted as "5 μM picrotoxin and 50 μM CGP54626."

Immunohistochemistry

The brain was dissected away from the head capsule and fixed for 14 minutes in 4% aqueous paraformaldehyde at room temperature. It was then washed in phosphate buffered saline (PBS) and incubated in blocking solution (5% goat serum in PBS + 0.2% Triton X-100 [PBST]) before being incubated in blocking solution containing primary antibodies (see below) for 24 hours at room temperature. Samples were washed again, this time in PBST, and then incubated in blocking solution containing secondary antibodies (see below) for another 24 hours at room temperature. Samples were then washed again in PBST before being mounted in Vectashield (Vector Laboratories) and visualized on a Zeiss LSM 510 or a Leica SP8 X laser-scanning confocal microscope.

To visualize the aPN3 neurons and C/E JONs in two different immunofluorescence channels (**Figure 1D**), we used the following genotype: *JO31-Gal4/ey-FLP;70G01-Gal4,UAS-CD2/UAS-FRT-stop-FRT-CD8:GFP*. In these flies, CD8:GFP was selectively expressed in C/E JONs by expressing FLP only in the antennae (using *ey-FLP*, Newsome et al., 2000) and a form of UAS-GFP containing a FRT-flanked stop codon (*UAS-FRT-stop-FRT-GFP*, Hong et al., 2009). Consequently, the aPN3 neurons expressed only CD2, and the C/E JONs expressed both CD2 and CD8:GFP. The primary antibody solution contained: mouse anti-CD2 (Serotec MCA-154GA) at 1:100, and rat anti-CD8 (Invitrogen MCD0800) at 1:50. The secondary antibody solution contained: goat anti-mouse:AlexaFluor633 (Invitrogen) at 1:250, and goat anti-rat:AlexFluor488 (Invitrogen) at 1:250.

To visualize the aPN3 neurons and A/B JONs in two different immunofluorescence channels (**Figure 1E**), we used the following genotype: *70G01-LexA(attP40)/13xLexAop2-CD8:GFP(attP40);JO15-Gal4/UAS-CD2*. In these flies, CD2 was selectively expressed in JONs, and CD8:GFP was selectively expressed in aPN3 neurons. The primary antibody solution contained mouse anti-CD2 (Serotec MCA-154GA) at 1:250. The secondary antibody solution contained goat anti-mouse:AlexaFluor633 (Invitrogen) at 1:500. Fluorescence in the aPN3 neurons was visualized on the basis of GFP fluorescence without further immunofluorescent amplification.

To selectively label the aPN3 neuron dendrites with DenMark while labeling the entire neuron with CD8:GFP (**Figure S2**), we used the following genotype: *UAS-DenMark(attP40)/+;10xUAS-IVS-CD8:GFP(su(Hw)attP1),70G01-Gal4(attP2)/+*. The primary antibody solution contained: mouse anti-Bruchpilot (DSHB nc82-s) at 1:50, rat anti-CD8 (Invitrogen MCD0800) at 1:50, and rabbit anti-DsRed (Clontech 632496) at 1:500. The secondary antibody solution contained: goat anti-mouse:AlexaFluor633

(Invitrogen) at 1:500, goat anti-rat:AlexFluor488 (Invitrogen) at 1:250, and goat anti-rabbit:AlexaFluor568 at 1:250.

To visualize the central axonal projections of JONs expressing CD8:GFP (**Figure S3A**), we used a primary antibody solution containing mouse anti-Bruchpilot (DSHB nc82-s) at 1:50 and rat anti-CD8 (Invitrogen MCD0800). The secondary antibody solution contained goat anti-mouse:AlexaFluor633 (Invitrogen) at 1:500 and goat anti-rat:AlexFluor488 (Invitrogen) at 1:250. To visualize JONs in the second antennal segment expressing CD8:GFP (**Figure S3B**), we mounted antennae directly in Vectashield (Vector Laboratories) and imaged native GFP fluorescence.

Optogenetic stimulation

We used the following genotypes to express CsChrimson, a red-shifted version of channelrhodopsin, in JONs, while also expressing CD8:GFP in the aPN3 neurons:

Figure 1F: C/E JONs: *JO31-Gal4/20XUAS-IVS-CsChrimson.mVenus(attP40);10xUAS-IVS-CD8:GFP(su(Hw)attP1)/10xUAS-IVS-CD8:GFP(su(Hw)attP1),70G01-Gal4(attP2)*
Figure S4A: C/E JONs: *10xUAS-IVS-CD8:GFP(attP40)/20XUAS-IVS-CsChrimson.mVenus(attP40);60H03-Gal4(attP2)/10xUAS-IVS-CD8:GFP(su(Hw)attP1),70G01-Gal4(attP2)*
Figure S4B: A/B JONs: *10xUAS-IVS-CD8:GFP(attP40)/20XUAS-IVS-CsChrimson.mVenus(attP40);JO15-Gal4/10xUAS-IVS-CD8:GFP(su(Hw)attP1),70G01-Gal4(attP2)*

The last generation of each of these crosses was raised in foil-wrapped 6-oz culture bottles where the surface of the regular food was covered with ~1 cm layer of rehydrated potato flakes mixed with all-trans retinal (100 µL of a 35 mM solution in ethanol). Prior to each experiment, females of the appropriate age were selected and housed overnight in foil-wrapped culture vials containing potato food and 100 µL all-trans retinal.

To stimulate ipsilateral JONs, we connected a fiber optic (Thorlabs M87L01) to a cannula (Thorlabs FG050UGA) with a ceramic adapter (Thorlabs CFLC126-10) and coupled it to a green LED (Smart Vision Lights S30-530-F). We directed the fiber optic at the second antennal segment, where the JONs are housed, and visualized its alignment with respect to the second antennal segment using two different camera angles (as described above in Piezoelectric stimulation). We drove the LED using Matlab and a NI-DAQ analog output channel delivering a 6-V signal fluctuating at 100 Hz, with a duty cycle of 0.2 - 0.4 (0.276 - 0.720 µW).

In all of our flies, the aPN3 neurons also expressed CsChrimson. We found that these ChR-expressing aPN3 neurons were depolarized by around 5-10 mV when exposed to ambient room light. To prevent this, the electrophysiology set-up was surrounded by a black box during these experiments. The voltage command to the LED was adjusted (to approximately 0.5 µW) so that illumination of the antenna produced no more than 2 mV of direct excitation in aPN3 neurons (as assessed by the washing on 1 µM TTX at the end of the experiment and measuring the magnitude of the TTX-insensitive responses in aPN3 neurons).

Piezoelectric stimulation

All experiments using the piezoelectric actuator were performed with the probe attached to the ipsilateral antenna. Deflecting the contralateral antenna with the probe elicited no response in the aPN3 neurons. Half of the experiments used an open-loop piezoelectric actuator (Physik Instrumente P-840.60, 90 µm travel range, with E-505 amplifier and E-500 chassis). The other half used a closed-loop piezoelectric actuator (Physik Instrumente P-841.60, 90 µm travel range, with E-509.S1 sensor/piezo servo-control module).

When using the open-loop piezoelectric actuator, we butt-coupled two actuators of the same type in the opposite orientation in order to minimize mechanical oscillations after movement of the actuator. Identical probes were attached to both actuators in order to make them as balanced as possible. An iterative sculpting protocol was used to create voltage command signals to the piezoelectric actuators that would generate our desired displacement waveforms; here, a laser Doppler vibrometer was used to measure the movements of the piezoelectric actuator, and Matlab iteratively modified the command voltage until the actual displacement matched the desired displacement.

When using the closed-loop piezoelectric actuator, we employed a single actuator and monitored its movement using its built-in strain gauge sensor. Because the device operated in closed-loop, it could produce arbitrary displacement waveforms without using the sculpting protocol described above.

For all experiments using piezoelectric actuators, stimuli were generated in software (Matlab) at a sample rate of 10 kHz, and sent to the Physik Instrumente amplifiers. The actuator was coupled to the fly's arista via a stiff probe fabricated using a tungsten microelectrode (Microprobes WE5PT31.5A10) that was cut to be about 3 cm (preserving the tip) and then threaded through a glass capillary (1.5 mm outer diameter) filled with UV-curable glue. This probe was attached to the actuator using a cylindrical aluminum housing with an M3 set screw on one end that could be screwed into the actuator. The cylindrical housing extended more than halfway up the probe in order to increase its stiffness. The probe was attached to the most distal branch point of the arista, and a tiny drop of gasket sealant (Loctite Gasket Sealant 2) was placed on the tip of the probe in order to create tight adhesion with the arista.

In order to ensure that the probe was inducing purely rotational movement of the antenna (i.e., rotation about the antenna's long axis), we visualized the antenna and the probe using two video cameras placed at different angles and fitted with magnifying lenses. One camera was positioned directly beneath the fly, providing an approximately *en face* view of the arista, and the other was positioned to the side of the fly, providing a profile view of the antenna. We marked the position of the antenna and probe at the start of the experiment and monitored the image periodically in order to ensure that there was no drift during the course of the experiment.

Acoustic stimulation

Acoustic stimuli were delivered with a speaker (Scan-Speak Discovery 10F/4424G) that was positioned approximately 14 cm from the fly at an angle of approximately 45° with respect to the longitudinal axis of the fly, so that sound energy was directed at an angle perpendicular to the arista. The speaker was always aimed at the arista that was ipsilateral to the aPN3 neuron being recorded (because aPN3 neurons do not receive inputs from the contralateral antenna, data not shown). Sound waveforms were generated in Matlab at a sample rate of 40 kHz and then delivered to the speaker via a NI-DAQ analog output channel and a Crown D-45 amplifier. Sound intensity (in particle velocity) at the position of the fly was measured as ~ 20 mm/s using a calibrated particle velocity microphone (Knowles Electronics NR-23158). See Lehnert et al. (2013) for details on microphone calibration.

In order to prevent the speaker from causing the air table (and the electrophysiology set-up) to vibrate, we decoupled the speaker from the air table. The speaker was attached to a magnetic base, which was then attached to a magnetic plank clamped to the frame of the air table. The speaker and its wiring were enclosed in a grounded copper mesh cage in order to reduce electrical noise. We confirmed that removing the antennae abolished all sound responses in aPN3 neurons, indicating that mechanosensitive neurons in other organs are not the source of the aPN3 neuron sound response.

Laser Doppler vibrometry and fictive wind stimulus

Wind-driven antennal movements were measured using a laser Doppler vibrometer (Polytec OFV-5000 equipped with OFV-500, VD-06, and DD-500 decoder boards). A particle velocity microphone was placed within 1 cm of the fly, so that the stimulus and the mechanical response of the antenna were simultaneously recorded and acquired in Matlab. We used an array of six fans (3 inch diameter, Rosewill RFA-80-K, Model DFS802512M) to generate a turbulent wind stimulus with an average wind speed of 0.4 m/s, a speed that flies have been observed to experience in a natural environment (Budick and Dickinson, 2006). The fly was placed in a trimmed 200 µL micropipette tip, and its legs and proboscis were restrained with paraffin wax. UV-curable glue was used to fix the head to the body and the second antennal segment to the head. This removed voluntary movements of the head and antennae. The micropipette tip was mounted on a micromanipulator and was visualized using a CCD video imaging system coupled to a 15× objective (Edmund Optics 58418). The laser measurement spot was placed at the base of the arista.

We then used these measurements of wind-evoked antennal movements to generate fictive wind stimuli with the piezoelectric actuator having similar frequency and amplitude content. Specifically, segments of random Gaussian noise were generated and filtered so that the power spectrum of the random waveforms resembled that of wind-evoked antennal movements (most energy was below 200 Hz). The amplitude of the white noise stimulus was chosen to resemble the displacement magnitudes evoked by the turbulent wind stimulus (standard deviation of 2.35 µm). Although the wind stimulus occasionally evoked large, high-frequency 20 µm bursts in antennal movement, we chose to omit these types of movements from the fictive wind stimulus because piezoelectric movements this large tended to produce non-rotational movement of the antenna.

Statistics and data analysis

Sample sizes were qualitatively determined by the observed cell-to-cell reliability in the measurements we performed in pilot experiments. Our sample sizes are similar to those generally employed in the field. Data distribution was assumed to be normal, but this was not quantitatively determined. No blinding was performed during experiments or analysis.

All data analysis was carried out in Matlab. Measurements of membrane potential were downsampled to 1 kHz before analysis and averaging. Spikes were detected by differentiating the voltage trace and marking fluctuations that passed a certain threshold (determined by eye and adjusted as needed). All spikes were automatically detected in this manner and then individually verified by eye; spurious spikes were removed and missed spikes were added. In all the traces shown in the figures that are denoted as "average voltage", spikes were clipped (prior to trial-averaging of the voltage traces) by setting the values in a 10-ms window centered at a detected spike time point equal to the value at 5 ms before the spike time point. The 10 ms window width was chosen because this is the spike width near the base of most spikes (aPN3 neuron spikes are generally stereotyped in shape and time course). This spike clipping procedure reliably decreased spike amplitudes by 60-80%. After spikes were clipped, voltage was averaged across all presentations of the same stimulus for that cell.

When a figure shows multiple example neurons, each neuron was recorded in a different fly. Examples were chosen to be representative of the types of responses seen within each data set.

Modeling

All modeling was carried out in Matlab. JON responses to a given antennal displacement were specified by sigmoid displacement-response curves. The two JON subgroups (push and pull) were defined by a pair of mirror-image displacement-response curves (**Figure 5A**). We follow the convention of specifying the rotational movement of the antenna in terms of the displacement (x) that this rotation causes at a distal point on the arista. The time-dependent response $r(t)$ of the push JONs was given a sigmoid function of displacement:

$$r(t) = \alpha \frac{1}{1+e^{(\beta x(t)+s(t)+\gamma)}} + \delta \qquad \text{Eq. 1}$$

Displacement ($x(t)$) is zero at the antenna's normal resting position, positive for movements toward the head, and negative for movements away from the head. We chose to model responses as a sigmoid function of displacement (rather than log displacement) following Effertz et al. (2012). Although several earlier studies described JON responses as a sigmoid function of log displacement (Effertz et al., 2011; Kamikouchi et al., 2009; Lehnert et al., 2013; Yorozu et al., 2009), the measurements in these studies do not clearly discriminate between the two possibilities. We also confirmed that we could capture the key features of aPN3 neuron responses by modeling JON responses as a sigmoid function of log displacement.

In Eq. 1, term γ specifies the horizontal position of the sigmoid relative to the resting position of the antenna ($x = 0$). The term $s(t)$ causes this horizontal position to shift gradually after the antenna is displaced, thereby producing adaptation in JON responses. Following a displacement away from rest, $s(t)$ exponentially approaches a value equal to 25% of the displacement, with a time constant of 500 ms. Parameters for push JONs were set as follows: $\alpha = 100$, $\beta = -0.5$, $\gamma = 1.4$, $\delta = 0$. Parameters for pull JONs were: $\alpha = -100$, $\beta = -0.5$, $\gamma = -1.4$, $\delta = 100$.

The output of each sigmoid curve was low-pass filtered by convolving it with an integrating filter (an alpha function, **Figure 5A**):

$$y = \frac{\alpha}{\tau} t\, e^{(1-\frac{t}{\tau})} \qquad \text{Eq. 2}$$

In Eq. 2, term α represents the maximum amplitude of the alpha function, and τ represents the time constant. These parameters were set to $\alpha = 1\ \text{s}^{-1}$, and $\tau = 0.023$ s.

To obtain the inhibitory versions of each JON signal (i.e., to model inhibition driven by each JON type), the push and pull JON signals were bandpass filtered by convolving the output of the excitatory channel with a differentiating (biphasic) filter (**Figure 5A**). This biphasic filter was generated by taking the difference of an alpha function and a Gaussian. The alpha function is given in Eq. 2, and the parameters were set to $\alpha = 1\ \text{s}^{-1}$, and $\tau = 0.005$ s. The Gaussian function is as follows:

$$y = \alpha\, e^{\frac{-(t-\mu)^2}{2\sigma^2}} \qquad \text{Eq. 3}$$

The parameters were set to $\alpha = 0.65$, $\mu = 0.021$ s, $\sigma = 0.006$ s. To calculate the biphasic filter, the Gaussian function was subtracted from the alpha function.

This filter has a negative integral (**Figure 5A**), and so inhibitory inputs were sign reversed relative to the excitatory outputs. Both the integrating filter and the differentiating filter were hand-tuned to qualitatively fit the data. All inputs were summed linearly to generate a model of the aPN3 neuron membrane potential. Different model aPN3 neurons were generated by varying the weights on the three inputs (push+, pull-, push-).

In the version of the model where we explicitly modeled spiking behavior (**Figure 8B**), we generated the spike rate of each neuron by convolving the membrane potential with a biphasic filter. We found that the spike rates of real aPN3 neurons depended on not just the absolute membrane potential, but also the rate of change of the membrane potential (data not shown), and a biphasic filter was needed in order to capture this behavior. We generated this filter by taking the difference of an alpha function (Eq. 2) and a Gaussian (Eq.3). The parameters for the alpha function were set to $\alpha = 1.8\ \text{s}^{-1}$, and $\tau = 0.002$ s. The parameters for the Gaussian were set to $\alpha = 12.55$, $\mu = 0.79$ s, $\sigma = 0.002$ s. To calculate the biphasic filter, the Gaussian function (Eq. 3) was subtracted from the alpha function (Eq. 2).

This filter was scaled so that peak and spontaneous firing rates were realistic, and the firing rate was constrained to have a maximum of 60 Hz. The time-varying firing rate of each aPN3 neuron was then used to generate a Poisson-distributed spike train.

The goal of the models in this study was to recapitulate certain qualitative aspects of the biological data, not to create a quantitatively accurate model of the aPN3 neurons. Consequently, all elements of the model were hand-tuned to fit the data, and we did not calculate the goodness of fit. We also examined the robustness of the model to variations in the values of the fitted parameters (**Figure S7**). Overall, the model output was relatively robust to variations of ±25% in any given parameter. The parameters that the model was most sensitive to were those specifying the shape and amplitude of the fast initial component of the biphasic filter (the alpha function component).

References for Supplemental Experimental Procedures

Budick, S.A., and Dickinson, M.H. (2006). Free-flight responses of Drosophila melanogaster to attractive odors. J. Exp. Biol. *209*, 3001-3017.

Chen, T.W., Wardill, T.J., Sun, Y., Pulver, S.R., Renninger, S.L., Baohan, A., Schreiter, E.R., Kerr, R.A., Orger, M.B., Jayaraman, V.*, et al.* (2013). Ultrasensitive fluorescent proteins for imaging neuronal activity. Nature *499*, 295-300.

Effertz, T., Wiek, R., and Gopfert, M.C. (2011). NompC TRP channel is essential for Drosophila sound receptor function. Curr. Biol. *21*, 592-597.

Effertz, T., Nadrowski, B., Piepenbrock, D., Albert, J.T., and Gopfert, M.C. (2012). Direct gating and mechanical integrity of Drosophila auditory transducers require TRPN1. Nat. Neurosci. *15*, 1198-1200.

Gouwens, N.W., and Wilson, R.I. (2009). Signal propagation in Drosophila central neurons. J. Neurosci. *29*, 6239-6249.

Hong, E.J., and Wilson, R.I. (2015). Simultaneous encoding of odors by channels with diverse sensitivity to inhibition. Neuron *85*, 573-589.

Kamikouchi, A., Shimada, T., and Ito, K. (2006). Comprehensive classification of the auditory sensory projections in the brain of the fruit fly Drosophila melanogaster. J. Comp. Neurol. *499*, 317-356.

Kamikouchi, A., Inagaki, H.K., Effertz, T., Hendrich, O., Fiala, A., Gopfert, M.C., and Ito, K. (2009). The neural basis of Drosophila gravity-sensing and hearing. Nature *458*, 165-171.

Klapoetke, N.C., Murata, Y., Kim, S.S., Pulver, S.R., Birdsey-Benson, A., Cho, Y.K., Morimoto, T.K., Chuong, A.S., Carpenter, E.J., Tian, Z.*, et al.* (2014). Independent optical excitation of distinct neural populations. Nat. Methods *11*, 338-346.

Kohl, J., Ng, J., Cachero, S., Ciabatti, E., Dolan, M.J., Sutcliffe, B., Tozer, A., Ruehle, S., Krueger, D., Frechter, S.*, et al.* (2014). Ultrafast tissue staining with chemical tags. Proc. Natl. Acad. Sci. U. S. A. *111*, E3805-3814.

Kwon, Y., Shen, W.L., Shim, H.S., and Montell, C. (2010). Fine thermotactic discrimination between the optimal and slightly cooler temperatures via a TRPV channel in chordotonal neurons. J. Neurosci. *30*, 10465-10471.

Lehnert, B.P., Baker, A.E., Gaudry, Q., Chiang, A.S., and Wilson, R.I. (2013). Distinct roles of TRP channels in auditory transduction and amplification in Drosophila. Neuron *77*, 115-128.

Liu, W.W., and Wilson, R.I. (2013). Glutamate is an inhibitory neurotransmitter in the Drosophila olfactory system. Proc. Natl. Acad. Sci. U. S. A. *110*, 10294-10299.

Mamiya, A., and Dickinson, M.H. (2015). Antennal mechanosensory neurons mediate wing motor reflexes in flying Drosophila. J. Neurosci. *35*, 7977-7991.

Marella, S., Fischler, W., Kong, P., Asgarian, S., Rueckert, E., and Scott, K. (2006). Imaging taste responses in the fly brain reveals a functional map of taste category and behavior. Neuron *49*, 285-295.

Matsuo, E., Yamada, D., Ishikawa, Y., Asai, T., Ishimoto, H., and Kamikouchi, A. (2014). Identification of novel vibration- and deflection-sensitive neuronal subgroups in Johnston's organ of the fruit fly. Front. Physiol. *5*, 179.

Matsuo, E., Seki, H., Asai, T., Morimoto, T., Miyakawa, H., Ito, K., and Kamikouchi, A. (2016). Organization of projection neurons and local neurons of the primary auditory center in the fruit fly Drosophila melanogaster. J. Comp. Neurol. *524*, 1099-1164.

Morley, E.L., Steinmann, T., Casas, J., and Robert, D. (2012). Directional cues in Drosophila melanogaster audition: structure of acoustic flow and inter-antennal velocity differences. J. Exp. Biol. *215*, 2405-2413.

Newsome, T.P., Asling, B., and Dickson, B.J. (2000). Analysis of Drosophila photoreceptor axon guidance in eye-specific mosaics. Development *127*, 851-860.

Nicolai, L.J., Ramaekers, A., Raemaekers, T., Drozdzecki, A., Mauss, A.S., Yan, J., Landgraf, M., Annaert, W., and Hassan, B.A. (2010). Genetically encoded dendritic marker sheds light on neuronal connectivity in Drosophila. Proc. Natl. Acad. Sci. U S A *107*, 20553-20558.

Pfeiffer, B., Ngo, T.-T.B., Hibbard, K.L., Murphy, C., Jenett, A., Truman, J.W., and Rubin, G.M. (2010). Refinement of tools for targeted gene expression in Drosophila. Genetics *186*, 735-755.

Pfeiffer, B.D., Jenett, A., Hammonds, A.S., Ngo, T.T., Misra, S., Murphy, C., Scully, A., Carlson, J.W., Wan, K.H., Laverty, T.R.*, et al.* (2008). Tools for neuroanatomy and neurogenetics in Drosophila. Proc. Natl. Acad. Sci. U. S. A. *105*, 9715-9720.

Sweeney, L.B., Couto, A., Chou, Y.H., Berdnik, D., Dickson, B.J., Luo, L., and Komiyama, T. (2007). Temporal target restriction of olfactory receptor neurons by Semaphorin-1a/PlexinA-mediated axon-axon interactions. Neuron *53*, 185-200.

Vaughan, A.G., Zhou, C., Manoli, D.S., and Baker, B.S. (2014). Neural pathways for the detection and discrimination of conspecific song in D. melanogaster. Curr. Biol. *24*, 1039-1049.

Vlasits, A.L., Bos, R., Morrie, R.D., Fortuny, C., Flannery, J.G., Feller, M.B., and Rivlin-Etzion, M. (2014). Visual stimulation switches the polarity of excitatory input to starburst amacrine cells. Neuron *83*, 1172-1184.

Wilson, R.I., and Laurent, G. (2005). Role of GABAergic inhibition in shaping odor-evoked spatiotemporal patterns in the Drosophila antennal lobe. J. Neurosci. *25*, 9069-9079.

Yorozu, S., Wong, A., Fischer, B.J., Dankert, H., Kernan, M.J., Kamikouchi, A., Ito, K., and Anderson, D.J. (2009). Distinct sensory representations of wind and near-field sound in the Drosophila brain. Nature *458*, 201-205.